Proceedings of the 48th National Conference on Fluid Mechanics and Fluid Power (FMFP)
December 27-29, 2021, BITS Pilani, Pilani Campus, RJ, India.

FMFP2021–05–145

On dynamic and heat transfer characteristics of elastically mounted heated circular cylinder undergoing VIV

Sambit Kumar Biswal[1]*, Prashant Kumar[2], Shaligram Tiwari[1]

[1]Department of Mechanical Engineering, Indian Institute of Technology Madras, Chennai, 600036, India
[2]Department of Mechanical Engineering, University of Tokyo, Tokyo, 153-8505, Japan
*Corresponding author: sambit775000@gmail.com

ABSTRACT

Numerical investigations are carried out in flow past spring-mounted heated circular cylinder undergoing vortex-induced vibrations. The computations are performed using Open Source Field Operations and Manipulation (OpenFoam). The existing solver has been modified to include thermal effects of the circular cylinder. Two degrees of freedom, i.e., the transverse and streamwise oscillations of the cylinder, are considered in the present study. The computations are carried out assuming a negligible damping ratio at Re values of 150 and 200. Wake characteristics are examined for different values of reduced velocity (U_r) varying from 3 to 8. The effect of U_r on cylinder displacement, lock-in behaviour, and frequency ratio is disclosed for the heated cylinder. Unsteady flow and thermal characteristics of the wake are illustrated using vorticity and temperature contours. The variation in the average value of Nusselt number around the cylinder has been plotted for different values of reduced velocity. Force coefficients on the cylinder surface are also reported for varying U_r.

Keywords: Vortex-induced vibration, reduced velocity, lock-in behaviour, frequency ratio, lift and drag coefficients.

1. INTRODUCTION

Investigations on flow past circular cylinder are carried out extensively by researchers and engineers due to its vast engineering applications. The complex wake structure is analyzed based on Reynolds number both experimentally and numerically. The shear layers become unstable, resulting in periodic shedding of vortices for Re $\geq$ 47 [1]. This causes unsteady forces on cylinder surface in the streamwise and transverse directions leading to vortex-induced vibrations (VIV). The VIV can be presented as the elastically mounted cylinder undergoing free vibrations due to the action of unsteady forces. For specific conditions, the wake shedding frequency may match the cylinder vibration frequency known as "lock-in" or "synchronization". The cylinder displacement attains maximum values in the lock-in regime, enhancing the wake complexity.

There are different parameters, such as mass ratio (m^*), damping ratio (ζ), Reynolds number (Re), and reduced velocity (U_r), that affect the VIV. Plenty of research is available to showing the influence of these parameters on cylinder response and wake characteristics. Feng [2] and Khalak and Williamson [3] studied cylinder response and branching behaviour in their experiments for flow past elastically mounted circular cylinder. They have reported three different response branches, viz., initial, upper and lower for smaller values of the combined mass-damping parameter ($m^*\zeta$). For smaller values of m^* and ζ, the shedding frequency differs from the structural frequency known as "soft lock-in" [3]. Blevins and Coughran [4] and Jauvtis and Williamson [5] examined VIV with two-degree-of-freedom in a steady flow and reported that the reduced velocity strongly affects the planar trajectory of the cylinder.

Govardhan and Williamson [6, 7] and Sanchis et al. [8] studied mode analysis of VIV with two-degree-of-freedom and reported that the response amplitude is governed by the so-called Skop–Griffin parameter. This parameter is proportional to the product of the mass and the damping [3, 6, 7]. Different vortex shedding modes have also been observed for cylinder undergoing VIV. Singh and Mittal [9] reported that a circular cylinder in free vibration with two degrees of freedom exhibits 2S mode at low Re, while it shows P + S mode at Re about 300 and above. The different vortex shedding regimes are classified and identified by Williamson and Roshko [10]. The 2P and P + S modes are reported for inline oscillation [11, 12] and transverse vibration [13]. Prasanth and Mittal [14] studied extensively VIV of the circular cylinder and examined phase and lock-in phenomena, cylinder response, and aerodynamic characteristics.

The aerodynamic and hydrodynamic characteristics of a cylinder undergoing VIV have been examined extensively and reported in literature. In numerous situations, the heat transfer features become an important aspect. For example, due to the aerodynamic forces on the heat exchangers tubes, the tubes may vibrate, leading to the change in heat transfer coefficient. In suc situation, heat transfer coefficient may become critical and must be examined. The heat transfer behavior are studied in detail for flow past stationary circular cylinder [15-19]. The effect of lock-in on convective heat transfer characteristics is investigated by Cheng et al. [20] for the transverse oscillation of the cylinder. Suppression of wake oscillation of a circular cylinder undergoing VIV considering mixed convection has been examined by Hasan and Ali [21]. The critical Richardson number for the onset of wake oscillation is reported by Hasan

S. Bhattacharyya and A. C. Benim (eds.), *Fluid Mechanics and Fluid Power (Vol. 2)*,
Lecture Notes in Mechanical Engineering, https://doi.org/10.1007/978-981-19-6970-6_38

and Ali [21] and Sengupta et al. [22]. Wan and Patnaik [23] studied the suppression of VIV using thermal buoyancy at Re equal to 150. The VIV of the heated cylinder has not been examined in detail. Therefore, the present study is motivated by such gaps in the literature dealing with the effect of reduced velocity and Re on VIV of the heated circular cylinder. The fluid is taken as air with a negligible damping coefficient at Re values of 150 and 200.

2. PROBLEM FORMULATION

Figure 1 shows the two-dimensional representation of the computational domain of an elastically mounted heated circular cylinder undergoing VIV placed inside a rectangular domain. Cylinder is located at a distance of 10D (L_u = 10D, where "D" is the diameter of the cylinder) from the inlet. Length and width of the computational domain are L_1 = 36D and L_2 = 20D. The Reynolds number (Re) is considered as 150 and 200.

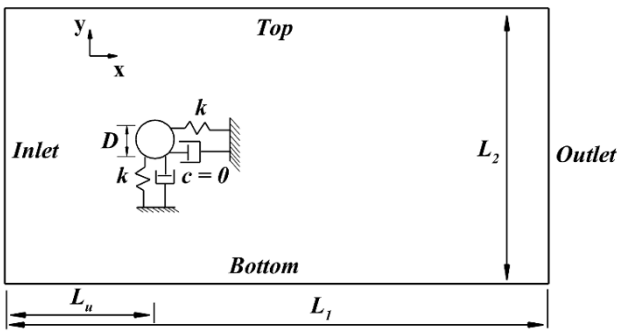

Figure 1: Schematic of the computational domain

3. GOVERNING EQUATIONS AND BOUNDARY CONDITIONS

Flow is considered to be two-dimensional and incompressible. Mass, momentum, and energy conservation equations are solved assuming unsteady and laminar. The non-dimensional governing equations can be given as

$$\frac{\partial U_i}{\partial X_i} = 0 \tag{1}$$

$$\frac{\partial U_i}{\partial t} + \frac{\partial U_i U_j}{\partial X_j} = -\frac{\partial P}{\partial X_i} + \frac{1}{\mathrm{Re}}\left(\frac{\partial^2 U_i}{\partial X_j \partial X_j}\right) \tag{2}$$

$$\frac{\partial \theta}{\partial t} + \frac{\partial \theta U_j}{\partial X_j} = \frac{1}{\mathrm{RePr}}\left(\frac{\partial^2 \theta}{\partial X_j \partial X_j}\right) \tag{3}$$

In a Cartesian coordinate system, velocity U_i denotes non-dimensional Cartesian velocity components U, V and W along X, Y and Z-directions respectively. Here $\theta = \frac{T-T_\infty}{T_w-T_\infty}$ is the non-dimensinal temperature. Reynolds number (Re) is defined as $\mathrm{Re} = \frac{U_\infty D}{\nu}$, where ν is the kinematic viscosity of the fluid and U_∞ and D are free-stream velocity and diameter of the cylinder, respectively. Prandtl number is defined as $\mathrm{Pr} = \frac{\mu C_p}{K}$, where μ, C_p and K are dynamic viscosity, specific heat capacity, and thermal conductivity of the fluid.

In the present study, a circular cylinder is flexibly mounted, and the cylinder movement is allowed in X- and Y-directions. Here, the structural damping ratio (ζ) is considered to be negligible and may result in large amplitude of oscillation. Cylinder motion in both directions is administered by the following equations expressed in non-dimensional form.

$$\ddot{X} + \frac{4\pi\zeta}{U_r}\dot{X} + \left(\frac{2\pi}{U_r}\right)^2 X = \frac{2Cd}{m^*} \tag{4}$$

$$\ddot{Y} + \frac{4\pi\zeta}{U_r}\dot{Y} + \left(\frac{2\pi}{U_r}\right)^2 Y = \frac{2Cl}{m^*} \tag{5}$$

where U_r is the reduced velocity, m^* is the mass ratio. Here Cd and Cl are the instantaneous drag and lift coefficients, respectively. Here, $\ddot{X}$, $\dot{X}$ and X indicate the normalized acceleration, velocity, and displacement of the cylinder in the streamwise direction, respectively. respectively. Reduced velocity (U_r) is defined as $U_r = \frac{U_\infty}{f_N D}$, where f_N is the natural frequency of the cylinder. Mass ratio (m^*, the ratio of mass of cylinder to that of the displaced fluid) can be expressed as $m^* = \frac{4m}{\pi\rho D^2}$, where m is the mass of the cylinder. In the present study, U_r is varied from 3.0 to 8.0 and m^* is fixed as 10.

Boundary conditions imposed on different surfaces can be given as.

Inlet: $U = U_\infty$, V = 0, $\frac{\partial P}{\partial X} = 0, T = T_\infty$

Outlet: $\frac{\partial U}{\partial X} = 0, \frac{\partial V}{\partial X} = 0, P = 0, \frac{\partial T}{\partial X} = 0$

Top and bottom: $\frac{\partial U}{\partial Y} = 0, \frac{\partial V}{\partial X} = 0, \frac{\partial P}{\partial Y} = 0, \frac{\partial T}{\partial Y} = 0$

Cylinder surface: $U = \dot{X}$, V = $\dot{Y}$, $\frac{\partial P}{\partial n} = 0, T = T_w$.

4. GRID AND NUMERICAL TECHNIQUE

The computational domain is divided into hexahedral grids with different blocks. Here O-grid with high grid density is created around the cylinder as shown in Figure 2. The grid density is reduced away from cylinder with a bi-geometric expansion ratio of less than 1.05. Grid convergence test is conducted at Re = 200 corresponding to different grid arrangements around the cylinder and near-wall cell size. The mean drag coefficient (Cd_{mean}) and maximum transverse displacement of the cylinder (Y_{max}) are reported in Table 1. The values of Cd_{mean} and Y_{max} decrease gradually with the increase in the number of divisions around the cylinder and reduce in the near-wall cell size. However, these changes are negligible as the total number of nodes changes from 64999 to 98664. Therefore, all the computations are performed considering 64999 as total number of nodes with 180 divisions around cylinder and 0.004 as first cell height.

Continuity, momentum, and energy equations are solved using Finite volume-based Open Source Field Operation and Manipulation (OpenFOAM) C++ library. PIMPLE algorithm has been used to resolve the coupling between pressure and velocity. Pressure and diffusive terms are discretized using a second-order accurate Gauss linear scheme, whereas a fourth-order Gauss cubic scheme is employed to discretize convective terms. The convective term in the energy equation is discretized using a bounded second-order Gauss linear scheme. First-order Euler implicit scheme is used to discretize the time derivatives term in momentum and energy equations. For pressure, velocity and temperature, absolute convergence criteria have been fixed as 10^{-7} in each iteration. Time step for computations has been

chosen in such a way that the maximum courant number falls below 0.5.

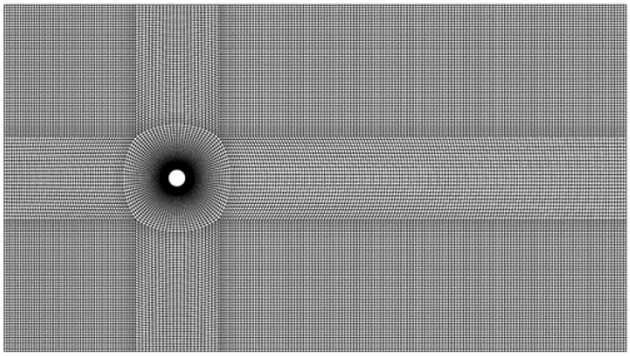

Figure 2: Grid arrangement

Table 1: Values of Cd_{mean} and Y_{max} for different grid arrangements

Total no of nodes (N)	No of divisions around cylinder (n)	Near wall grid size (Δr)	Cd_{mean}	Y_{max}
29894	100	0.013	2.013	0.552
43434	140	0.008	1.983	0.536
64999	**180**	**0.004**	**1.975**	**0.529**
98664	220	0.002	1.972	0.528

5. RESULTS AND DISCUSSION

5.1 Validation of Computations

Results are compared with those present in the literature. Table 2(a) compares the values of Y_{max} and X_{rms} at Re = 100 for U_r = 5 and 6 from the present study with those reported by Singh and Mittal [9]. The numerical results are in close match with those reported by Singh and Mittal [9] for corresponding to each U_r. Validation has been further extended to compare the Nusselt number (Nu) with the literature for a heated stationary cylinder at Re = 150, Pr = 0.7. The local Nussel number (Nu) and convective heat transfer coefficient (h) are related as

$$Nu = \frac{hD}{K} \tag{6}$$

The analytical expression for the variation in average Nusselt number ($\overline{Nu}$) with Re and Pr is given by Knudsen and Katz [24] (Eqn. 7). Table 2(b) shows that Nu matches closely with the analytical value and the Nu reported by Mahir and Altac [25].

$$\overline{Nu} = 0.683 Re^{0.466} Pr^{\frac{1}{3}} \tag{7}$$

Table 2: (a) comparison of Y_{max} and X_{rms} at Re = 200

Authors	U_r	Y_{max}	X_{rms}
Singh and Mittal [9]	5	0.561	0.006
	6	0.503	0.005
Present study	5	0.573	0.006
	6	0.505	0.004

(b) Value of Nusselt number (Nu) at Re = 150 and Pr = 0.7

	Mahir and Altac [25]	Analytical	Present study
Nu	6.38	6.26	6.40

5.2 Lock-in Regime

Figure 3 shows the Y_{max} and RMS value of streamwise displacement (X_{rms}) with the change in reduced velocity (U_r) at two different values of Re. The cylinder response, i.e., Y_{max} and X_{rms} increase initially with the sudden rise when U_r changes from 3.5 to 4.5. This is primarily caused by the shift from desynchronous to the synchronous regime. There appears a considerable variation in X_{rms} as compared to Y_{max} in the synchronous regime. The cylinder response is found to be maximum in the synchronous regime. At Re = 150, the values of Y_{max} and X_{rms} decrease after U_r = 6.5 due to a shift to desynchronous regime. On the other hand, at Re = 200, the synchronous regime gets narrower, and the values of Y_{max} and X_{rms} decrease after U_r = 5.5 as depicted in Fig. 3. The cylinder response (both in X- and Y-directions) is almost independent of U_r outside the synchronous regime. For a given value of U_r, Y_{max} is significantly higher than that of X_{rms} as shown in Fig. 3. For U_r = 4.5, Y_{max} is found to be 0.6, and the same value is reported in the literature [9]. With the change in Re, there appears a negligible change in the cylinder response up to the synchronous regime.

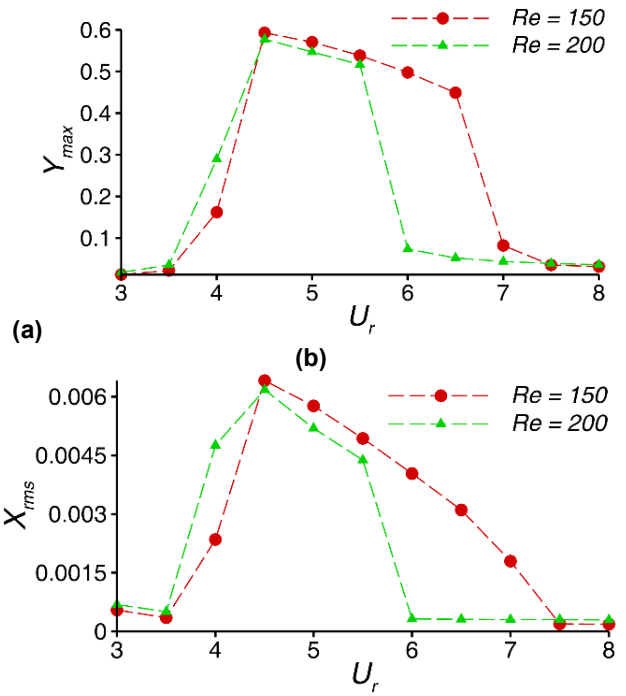

Figure 3: Variation in (a) Y_{max} and (b) X_{rms} with the change in U_r

Figure 4 shows the variation of frequency ratio, i.e., the ratio of cylinder oscillation frequency to that of the natural frequency of the structural oscillator (f/f_n) with the change in reduced

velocity U_r at Re values of 150 and 200. The synchronous/ lock-in regime is quite visible from the figure where the frequency ratio is close to 1. This regime is identified between 4.5 to 7.0, while it lies in 4.5 to 5.5 at Re values of 150 and 200, respectively. It is also confirmed from Fig. 3(a), in which a sudden jump in Y_{max} can be observed. In the synchronous regime, the wake oscillation frequency is noted to be equal to the cylinder oscillation frequency. In this regime, with the change in U_r, the natural frequency and cylinder oscillation frequency change in such a way that the frequency ratio remains the same. As we go away from the synchronous regime on either side, the cylinder oscillation frequency differs significantly from natural frequency. After lock-in regime, f/f_n varies linearly with U_r as shown in Fig. 4.

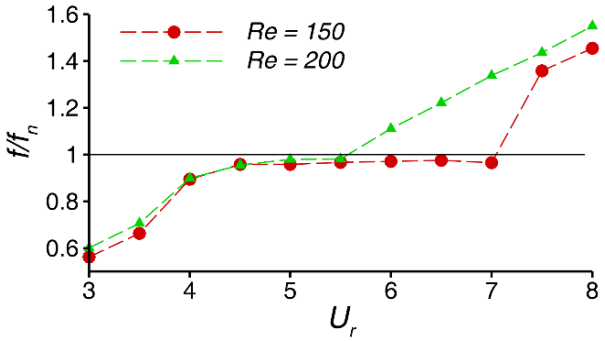

Figure 4: Variation of f/f_n with the change in U_r

5.3 Wake Flow

Figure 5 illustrates vorticity contours for different values of U_r at Re = 200. For brevity, the flow field behavior is not presented corresponding to Re = 150 due to the appearance of similar characteristics as observed at Re = 200. For $U_r < 4.5$, 2S mode of vortex shedding, i.e., two single vortices are shed in each shedding cycle, is observed. In this case, vortices are arranged alternatively in the wake region and appear to be of the similar arrangement as observed for stationary cylinder [1]. However, this pattern gets disturbed when the maximum amplitude of transverse vibration is observed (for $U_r = 4.5$). It can be seen that the vortices of similar sense of rotation coalesce on both sides in far wake, called as C(2S) mode of vortex shedding [9, 14]. Moreover, this formation gets delayed with an increase in U_r and seems to be completely absent for $U_r = 5.5$. With further increase in U_r, 2S wake pattern is observed as shown in Fig. 5. This reveals that only 2S vortex shedding mode is present in desynchronous regime.

5.4 Heat Transfer Characteristics

Figure 6 depicts the temperature contours for different values of U_r at Re = 200. The temperature contours resemble the vorticity contours. The periodic vortex shedding leads to the periodic behaviour of the temperature field. It can be observed that a longer length is required for temperature variation to disappear in the desynchronous regime as illustrated in Fig. 6. Therefore, U_r has a significant effect on temperature contours and, subsequently, energy transfer. The VIV affects the temperature gradient around the cylinder and hence the thermal energy transfer.

Figure 7 shows the variation in average Nusselt number ($\overline{Nu}$) with varying U_r at Re values of 150 and 200. For fixed Re, the $\overline{Nu}$ is higher in the synchronous regime and is almost independent of U_r in the desynchronous regime. It is found to be maximum (= 9.1) for $U_r = 4.5$ at Re = 200. At Re = 150 and 200, maximum value of $\overline{Nu}$ is corresponding to C(2S) mode of vortex shedding. The $\overline{Nu}$ decreases linearly in the synchronous regime with the increase in U_r. The $\overline{Nu}$ for the stationary cylinder is calculated as 6.26 and 7.16 from Eqn. (7) at Re values of 150 and 200, respectively. There is an overall increase in $\overline{Nu}$ for the cylinder undergoing VIV corresponding to each value of U_r compared to stationary cylinder. The difference is found to be maximum in synchronous regime. For fixed U_r, $\overline{Nu}$ is observed to be larger at a higher value of Re.

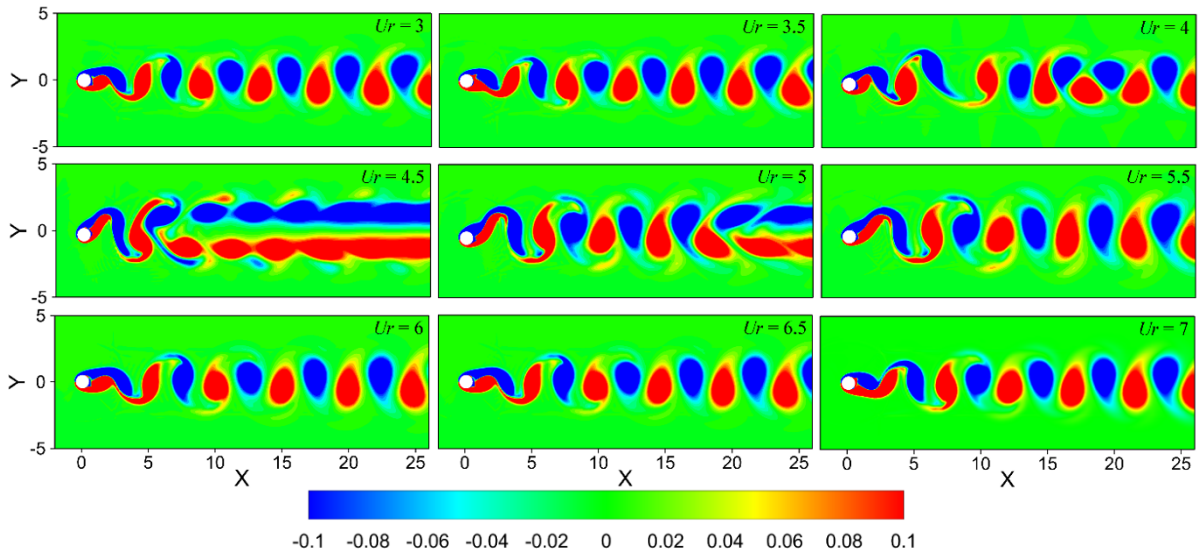

Figure 5: Wake structure for different values of U_r

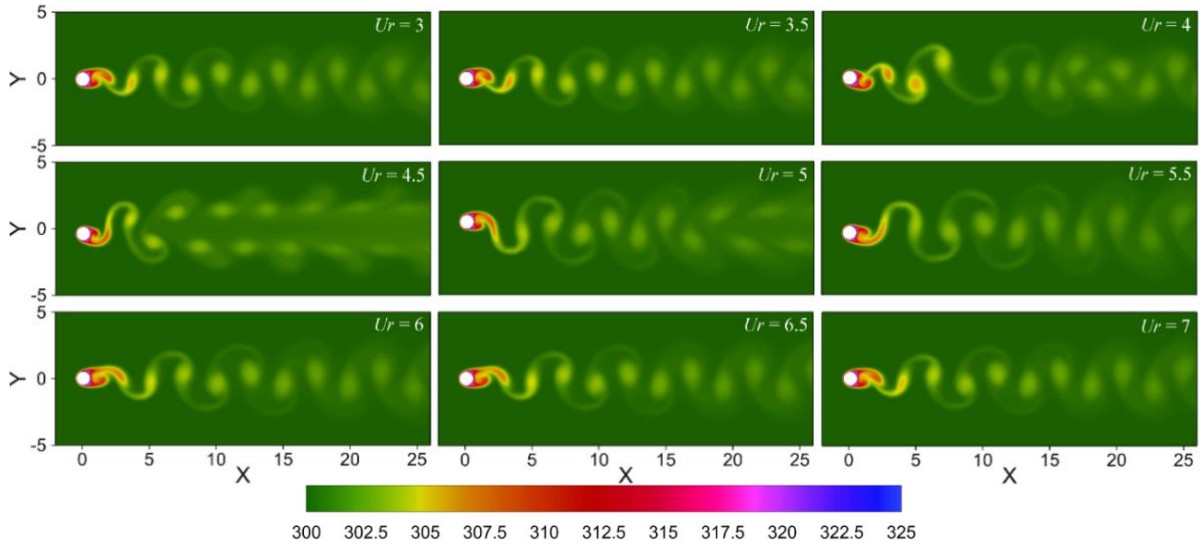

Figure 6: Temperature contours for different values of U_r

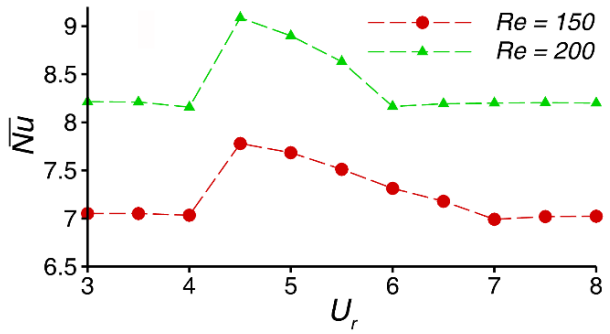

Figure 7: Variation in average Nusselt number ($\overline{Nu}$) with the change in U_r

5.5 Dynamic Characteristics

Figure 8 depicts the variation in Cd_{mean} and Cl_{rms} with varying U_r for different values of Re. The Cd_{mean} gradually increases up to U_r = 4.5 and then decreases in the synchronous regime. It remains unchanged for U_r in the range of 7 to 8 and 6 to 8 at Re value of 150 and 200, respectively. On the other hand, Cl_{rms} increases up to U_r = 4 and then decreases monotonically up to U_r value of 5.5 at Re = 200. The reduction in the value of Cl_{rms} can be observed up to U_r = 6.5 at Re = 150. With further increase in U_r, Cl_{rms} increases as illustrated in Fig. 8(b). The maximum values of Cd_{mean} and Cl_{rms} are found to be 2.35 and 1.05 for U_r values of 4.5 and 4, respectively. The minimum values of Cd_{mean} and Cl_{rms} are observed to be 1.05 and 0.02 for U_r values of 6 and 5.5, respectively. The Cd_{mean} reported in the synchronous regime is observed to be higher than that of the fixed circular cylinder [26] at Re = 200.

6. CONCLUSIONS

Two-dimensional numerical computations are carried out to examine the effect of reduced velocity (U_r) on flow and thermal wake characteristics in flow past heated circular cylinder undergoing vortex-induced vibration. The synchronous regime lies between U_r values of 4.5 to 7.0 and 4.5 to 5.5 at Re values of 150 and 200, respectively. The displacement of the cylinder is found to be maximum in this regime. The frequency ratio is close to 1 in the synchronous regime. 2S mode of vortex shedding has been observed for all the values of U_r except U_r = 4.5 at Re = 200. For U_r = 4.5, i.e., at the onset of synchronous regime, C(2S) mode of vortex shedding occurs. The temperature contours resemble the vorticity contours corresponding to each U_r. The average value of Nusselt number ($\overline{Nu}$) is found to be more than that of the stationary cylinder at Re = 150 and 200. The value of $\overline{Nu}$ increases with the increase in U_r and is found to be maximum in the synchronous regime. With the increase in U_r, the mean drag coefficient first increases and attains a maximum value at U_r = 4.5 and then decreases. The mean drag coefficient is found to be almost independent of U_r in the desynchronous regime.

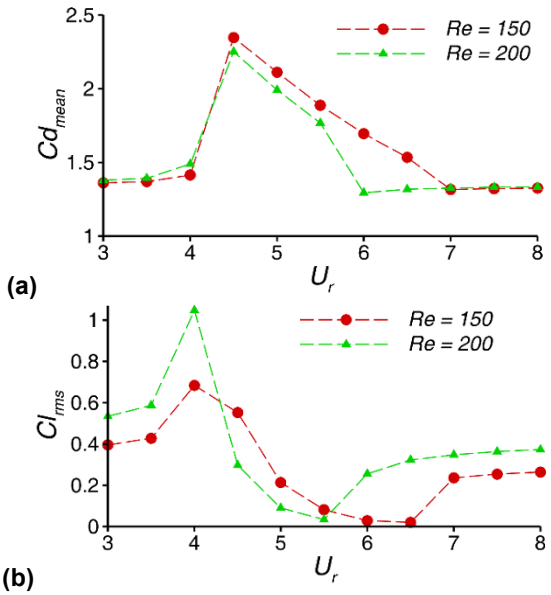

Figure 8: Variation in (a) Cd_{mean} and (b) Cl_{rms} with the change in U_r

NOMENCLATURE

Cd_{mean}	Mean drag coefficient (--)
Cl_{rms}	RMS value of lift coefficient (--)
f	Cylinder oscillation frequency (Hz)
f_n	Natural frequency of the structural oscillator (Hz)
K	Thermal conductivity of fluid (W/mK)
m	Mass of the cylinder (Kg)
m^*	Mass ratio (--)
$\overline{Nu}$	Time-averaged Nusselt number (--)
Pr	Prandtl number (--)
Re	Reynolds number (--)
U, V, W	Non-dimensionalized velocity component (--)
U_r	Reduced velocity (--)
U_∞	Free-stream velocity (m/s)
X, Y, Z	Non-dimensionalized Cartesian coordinates (--)
X_{rms}	RMS value of streamwise cylinder displacement (--)
Y_{max}	Amplitude of transverse cylinder oscillation (--)
ν	Kinematic viscosity (m^2/s)
ζ	Damping ratio (--)
ρ	Density (Kg/m^3)

REFERENCES

[1] C. H. K. Williamson, Vortex dynamics in the cylinder wake, Annual Review of Fluid Mechanics, 28, 1996, pp. 477-539.

[2] C. C. Feng, The Measurement of Vortex Induced Effects in Flow Past Stationary and Oscillating Circular and d Section Cylinders, Master's Thesis, Department of Mechanical Engineering, the University of British Columbia, Canada, 1968.

[3] A. Khalak, and C. H. K. Williamson, Motions, forces and mode transitions in vortex-induced vibrations at low mass-damping, Journal of Fluids and Structures, 13, 1999, pp. 813-851.

[4] R. D. Blevins, and C. S. Coughran, Experimental investigation of vortex-induced vibration in one and two dimensions with variable mass, damping, and Reynolds number, Journal of Fluid Engineering, 131, 2009, 101202.

[5] N. Jauvtis, and C. H. K. Williamson, The effect of two degrees of freedom on vortex-induced vibration at low mass and damping, Journal of Fluid Mechanics, 509, 2004, pp. 23-62.

[6] R. Govardhan, and C. H. K. Williamson, Modes of vortex formation and frequency response for a freely-vibrating cylinder, Journal of Fluid Mechanics, 420, 2000, pp. 85 130.

[7] R. Govardhan, and C. H. K. Williamson, Defining the 'modified Criffin plot' in vortex-induced vibration: revealing the effect of Reynolds number using controlled damping, Journal of Fluid Mechanics, 561, 2006, pp. 147 -180.

[8] A. Sanchis, G. Sælevik, and J. Grue, Two-degree-of freedom vortex-induced vibrations of a spring-mounted rigid cylinder with low mass ratio, Journal of Fluids and Structures, 24, 2008, pp. 907-919.

[9] S. P. Singh, and S. Mittal, Vortex induced oscillations at low Reynolds numbers: hysteresis & vortex-shedding modes, Journal of Fluids and Structures, 20, 2005, pp. 1085-1104.

[10] C. H. K. Williamson, and A. Roshko, Vortex formation in the wake of an oscillating cylinder, Journal of Fluids and Structures, 2, 1988, pp. 355-381.

[11] O. M. Griffin, and S. E. Ramberg, Vortex shedding from a cylinder vibrating in line with an incident uniform flow, Journal of Fluid Mechanics, 75, 1976, pp. 257-271.

[12] A. Ongoren, and D. Rockwell, Flow structure from an oscillating cylinder. Part 2. Mode competition in the near wake, Journal of Fluid Mechanics, 191, 1988, pp. 225 245.

[13] R. Zdera, O. F. Turan, and D. G. Havard, Towards understanding galloping: near-wake study of oscillating smooth and stranded circular cylinders in forced motion, Experimental Thermal and Fluid Science, 10, 1995, pp. 28-43.

[14] T. K. Prasanth, and S. Mittal, Vortex-induced vibrations of a circular cylinder at low Reynolds numbers, Journal of Fluid Mechanics, 594, 2008, pp. 463-491.

[15] Y. Hadad, and K. Jafarpur, Laminar forced convection heat transfer from isothermal cylinders with active ends and different aspect ratios in axial air flows, Heat and Mass Transfer, 47, 2011, pp. 59-68.

[16] Y. Hadad, and K. Jafarpur, Laminar forced convection heat transfer from isothermal bodies with unity aspect ratio in coaxial air flow, Heat Transfer Engineering, 33, 2012, pp. 245-254.

[17] V. K. Patnana, R. P. Bharti, and R. P. Chhabra, Two dimensional unsteady forced convection heat transfer in power-law fluids from a cylinder, International Journal of Heat and Mass Transfer, 53, 2010, pp. 4152-4167.

[18] N. I. Mikheev, V. M. Molochnikov, A. N. Mikheev, and O. A. Dushina, Hydrodynamics and heat transfer of pulsating flow around a cylinder, International Journal of Heat and Mass Transfer, 109, 2017, pp. 254-265.

[19] R. D. Selvakumar, and S. Dhinakaran, Forced convective heat transfer of nano-fluids around a circular bluff body with the effects of slip velocity using a multi-phase mixture model, International Journal of Heat and Mass Transfer, 106, 2017, pp. 816-828.

[20] C. H. Cheng, J. L. Hong, and W. Aung, Numerical prediction of lock-on effect on convective heat transfer from a transversely oscillating circular cylinder, International Journal of Heat and Mass Transfer, 40, 1997, pp. 1825-1834.

[21] N. Hasan, and R. Ali, Vortex-shedding suppression in two-dimensional mixed convective flows past circular and square cylinders, Physics of Fluids, 25, 2013, 053603.

[22] T. K. Sengupta, K. Venkatasubbaiah, and S. S. Pawar, Nonlinear instability of mixed convection flow over a horizontal cylinder, Acta Mechanical, 201, 2008, pp. 197 210.

[23] H. Wan, and S. S. Patnaik, Suppression of vortex-induced vibration of a circular cylinder using thermal effects, Physics of Fluids, 28, 2016, 123603.

[24] J. D. Knudsen, and D. L. Katz, Fluid dynamics and heat transfer, McGraw-Hills, New York, USA, 1958.

[25] N. Mahir, Z. Altac, Numerical investigation of convective heat transfer in unsteady flow past two cylinders in tandem arrangements, International Journal of Heat and Fluid Flow, 29, 2008, pp. 1309-1318.

[26] S. Behara, and S. Mittal, Wake transition in flow past a circular cylinder, Physics of Fluids, 22, 2010, 114104.